Driving-induced multiple $\mathcal{PT}$-symmetry breaking transitions and reentrant localization transitions in non-Hermitian Floquet quasicrystals

Longwen Zhou* and Wenqian Han
College of Physics and Optoelectronic Engineering, Ocean University of China, Qingdao 266100, China

(Received 15 March 2022; accepted 5 August 2022; published 12 August 2022)

The cooperation between time-periodic driving fields and non-Hermitian effects could endow systems with distinctive spectral and transport properties. In this paper, we uncover an intriguing class of non-Hermitian Floquet matter in one-dimensional quasicrystals, which is characterized by the emergence of multiple driving-induced $\mathcal{PT}$-symmetry breaking/restoring transitions, mobility edges, and reentrant localization transitions. These findings are demonstrated by investigating the spectra, level statistics, inverse participation ratios, and wave-packet dynamics of a periodically quenched nonreciprocal Harper model. Our results not only unveil the richness of localization phenomena in driven non-Hermitian quasicrystals but also highlight the advantage of the Floquet approach in generating unique types of nonequilibrium phases in open systems.

DOI: 10.1103/PhysRevB.106.054307

I. INTRODUCTION

Periodic driving fields could create dynamical states of matter that are absent in equilibrium settings, with Floquet topological phases [1–5] and discrete time crystals [6–10] being two representative examples. The discovery of these unique phases not only extends the classification of quantum matter to nonequilibrium situations [11–19] but has also led to breakthroughs in the experimental characterization of quantum dynamics in complex systems [20–33].

In recent years, possible new phases that could emerge due to the interplay between Floquet drivings and non-Hermitian effects have been considered. Theoretical progress has been made in the discovery of *non-Hermitian Floquet* topological insulators [34–44], second-order topological phases [45,46], topological superconductors [47,48], and semimetals [49–52]. Intriguing features such as non-Hermiticity induced Floquet topological edge states [45] and their coexistence with Floquet non-Hermitian skin effects [41] have also been uncovered. In experiments, setups like cold atoms [53] and photonics [54–58] have been demonstrated as efficient platforms to explore phases and transitions in driven non-Hermitian systems. Beyond the clean limit, high-frequency driving fields have been found as a flexible knob to control the spectral, localization, and topological transitions in non-Hermitian quasicrystals (NHQCs) [59]. However, the main power of Floquet engineering in generating unique nonequilibrium phases, which usually displays itself at resonant driving frequencies and amplitudes, has yet to be unveiled for non-Hermitian disordered systems.

A non-Hermitian static system described by a $\mathcal{PT}$-symmetric Hamiltonian H can undergo a $\mathcal{PT}$ transition when the energy spectrum of H switches from real to complex (or vice versa) with the change of system parameters. On one side of the transition point, all the eigenvalues of H are real and the system is in a $\mathcal{PT}$-invariant (unbroken) phase with all eigenstates being $\mathcal{PT}$ symmetric. On the other side of the transition point, certain eigenenergies have nonvanishing imaginary parts and the system is in a $\mathcal{PT}$-broken phase, in which certain eigenstates are not $\mathcal{PT}$ symmetric. Comparatively, a Floquet system can undergo a $\mathcal{PT}$ transition when the quasienergy spectrum of the system's Floquet operator U goes from real to complex (or vice versa) with the change of system parameters. On one side of the transition, all the quasienergies E of U obtained from the eigenvalue equation $U|\psi\rangle = e^{-iE}|\psi\rangle$ are real and the system is in a $\mathcal{PT}$-invariant (unbroken) phase with all Floquet eigenstates $|\psi\rangle$ being $\mathcal{PT}$ symmetric. On the other side of the transition, certain quasienergies of U have nonvanishing imaginary parts and the system is in a $\mathcal{PT}$ broken phase with certain non-$\mathcal{PT}$-symmetric Floquet eigenstates. The $\mathcal{PT}$ transition now shows up in the quasienergy spectrum of a Floquet operator instead of the energy spectrum of a Hamiltonian.

In the present paper, we show that going beyond high-frequency modulations, periodic driving fields could endow NHQCs with multiple $\mathcal{PT}$ spectral transitions, reentrant localization transitions, richer phase diagrams, and unique dynamical properties. These facts are demonstrated explicitly in a periodically quenched nonreciprocal Harper model (NRHM), as introduced in Sec. II. In Sec. III, we provide a theoretical framework to study the spectrum and transport properties of one-dimensional (1D) non-Hermitian Floquet quasicrystals. These methods are then applied to characterize the extended, critical, localized phases and the sequence of $\mathcal{PT}$ and localization transitions among them in the periodically quenched NRHM in Sec. IV. Wave-packet dynamics is further employed as a probe to signify non-Hermitian Floquet quasicrystals with different transport natures. The physical origins of rich non-Hermitian Floquet quasicrystal phases and transitions are discussed in Sec. V. We summarize our results and discuss potential future directions in Sec. VI. Some other numerical details are presented in Appendices A and B.

*zhoulw13@u.nus.edu

II. MODEL

NHQCs form a class of matter with a unique spectral, transport, and topological nature due to the interplay between lattice quasiperiodicity and non-Hermitian effects [60–74]. In this section, the setting of a periodically quenched NRHM is introduced, which is originated from a prototypical model in the study of NHQC.

The Hamiltonian of the static NRHM takes the form $\hat{H} = \hat{K} + \hat{V}$, where in the lattice basis $\{|n\rangle\}$ we have

$$\hat{K} = J\sum_n (e^{\gamma}|n\rangle\langle n+1| + e^{-\gamma}|n+1\rangle\langle n|), \tag{1}$$

$$\hat{V} = V\sum_n \cos(2\pi\alpha n)|n\rangle\langle n|. \tag{2}$$

Here $n \in \mathbb{Z}$ is the lattice index. $Je^{\pm\gamma}$ are the nearest-neighbor hopping amplitudes. V is the amplitude of the on-site potential $V_n = V\cos(2\pi\alpha n)$. We assume $J, V > 0$ without loss of generality. When $\gamma \neq 0$, the hoppings from the right to left and from the left to right neighboring sites become asymmetric, yielding a non-Hermitian Hamiltonian ($\hat{H} \neq \hat{H}^{\dagger}$). Meanwhile, an irrational α makes the on-site potential quasiperiodic, leading to a 1D NHQC [75,76]. The spectrum of $\hat{H}$, obtained by solving the eigenvalue equation $\hat{H}|\psi\rangle = E|\psi\rangle$ can be real in certain parameter regions due to the $\mathcal{PT}$ symmetry. To see this, we first take the periodic boundary condition (PBC) for $\hat{H}$ and the rational approximation $\alpha \simeq p/q$ for α. For example, if we set $\alpha = (\sqrt{5}-1)/2$, p and q can take two adjacent numbers in the Fibonacci sequence (with $p < q$) to form the rational approximation $\alpha \simeq p/q$. Applying the discrete Fourier transformation $|n\rangle = \frac{1}{\sqrt{L}}\sum_{l=1}^{L}|l\rangle e^{i2\pi\alpha ln}$ to $\hat{H}$ [63], we obtain its representation in momentum space as $\hat{H}' = \frac{V}{2}\sum_l(|l\rangle\langle l+1| + \text{H.c.}) + 2J\sum_l \cos(2\pi\alpha l + i\gamma)|l\rangle\langle l|$. Note that the quasimomentum here is $2\pi\alpha l$ and the length of lattice is $L = q$. We can now identify in momentum representation the $\mathcal{P}$ symmetry of the system as $\mathcal{P} = \sum_l |-l\rangle\langle l|$ and the $\mathcal{T}$ symmetry as the complex conjugate $\mathcal{K}$. The off-diagonal part of $\hat{H}'$ is Hermitian and clearly symmetric under the combined $\mathcal{PT}$ operation. The diagonal elements $W_n = 2J\cos(2\pi\alpha l + i\gamma)$ satisfy $W_n = W_{-n}^*$, which guarantees the invariance of the diagonal part of $\hat{H}'$ under the $\mathcal{PT}$ operation. Putting together, we have $[\mathcal{PT}, \hat{H}'] = 0$. The momentum-space representation of the system Hamiltonian $\hat{H}$ is thus symmetric under $\mathcal{PT} = \sum_l |-l\rangle\langle l|\mathcal{K}$. Going back to the lattice representation, we may express the $\mathcal{PT}$ symmetry operator as $\mathcal{PT} = (\sum_n |-n\rangle\langle n|)(\mathcal{K}U_{\text{FT}})$, where the Fourier transformation U_{FT} has the matrix elements $(U_{\text{FT}})_{n,l} = \frac{1}{\sqrt{L}}e^{-i2\pi\alpha nl}$. In fact, as $\hat{H}$ and $\hat{H}'$ only differ by a unitary Fourier transformation that is independent of the system parameters (J, V, γ), their spectra are identical under the PBC. The $\mathcal{PT}$-breaking transitions in the spectrum of $\hat{H}'$ are thus coincident with the real-to-complex spectrum transitions in $\hat{H}$. For example, with the increase of γ, the non-Hermitian effects become stronger and complex eigenenergies of $\hat{H}$ start to appear after the system undergoes the $\mathcal{PT}$-breaking transition. Under the PBC, such a transition was found to occur at $\gamma = \gamma_c = -\ln(2J/V)$ for $V > 2J > 0$ [75]. Interestingly, when γ changes from $\gamma_c + 0^+$ to $\gamma_c - 0^+$, the energies of all eigenstates change from complex to real and their spatial profiles switch from extended to localized with the common Lyapunov exponent (inverse localization length) $\lambda = \ln[Ve^{-\gamma}/(2J)]$ [75]. Therefore, we obtain a $\mathcal{PT}$ transition in conjunction with a localization transition for all eigenstates at a finite amount of hopping asymmetry $\gamma = \gamma_c$ in the NRHM. With Floquet periodic drivings, the $\mathcal{PT}$ transition points in the NRHM can be flexibly controlled [59]. Alternating transitions between extended and localized phases with distinct topological nature can be further induced via changing the driving field parameters. However, no mobility edges and intermediate phases are found in the presence of high-frequency driving fields [59].

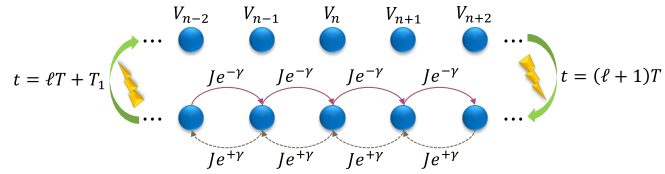

FIG. 1. Schematic plot of the periodically quenched nonreciprocal Harper model. In the upper chain, $V_n = V\cos(2\pi\alpha n)$ is the potential on the nth lattice site, which is spatially quasiperiodic for an irrational α. $Je^{\mp\gamma}$ couple nearest sites of the lower chain in an asymmetric manner when $\gamma \neq 0$. Within each driving period $T = T_1 + T_2$, the configuration of the system is switched between the upper and lower chains following the quench protocol described by Eq. (3). $\ell \in \mathbb{Z}$ counts the number of driving periods.

In this paper, we focus on a periodically quenched variant of the NRHM, which goes beyond the fast modulation protocol considered in previous studies [59]. The time-dependent Hamiltonian of the periodically quenched NRHM takes the form

$$\hat{H}(t) = \begin{cases} \hat{K} & t \in [\ell T, \ell T + T_1) \\ \hat{V} & t \in [\ell T + T_1, \ell T + T_1 + T_2). \end{cases} \tag{3}$$

Here $T = T_1 + T_2$ is the driving period. $\ell \in \mathbb{Z}$ counts the number of periods in the evolution. $\hat{K}$ and $\hat{V}$ are given by Eqs. (1) and (2), respectively. An illustration of this time-dependent lattice and the driving protocol is given in Fig. 1. The Floquet operator of the system, which corresponds to its evolution operator over a complete driving period reads

$$\hat{U} = e^{-i\mathsf{V}\sum_n \cos(2\pi\alpha n)|n\rangle\langle n|}e^{-i\mathsf{J}\sum_n(e^{\gamma}|n\rangle\langle n+1| + e^{-\gamma}|n+1\rangle\langle n|)}. \tag{4}$$

Here we have introduced the dimensionless parameters $\mathsf{V} = VT_2/\hbar$ and $\mathsf{J} = JT_1/\hbar$, with $\hbar$ being the Planck's constant. As an advantage of Floquet engineering, the amplitudes of hopping and onsite potential can be easily and separately tuned by varying the time durations T_1 and T_2 of the piecewise quench protocol, making it more flexible to control spectral and localization transitions in the system. Note that such a Floquet operator can also be realized by making the hopping amplitudes asymmetric in the kicked Harper model (KHM) [77–79]. The latter has been found to possess rich Floquet topological insulating phases in the Hermitian regime [80–82]. We can thus regard the Floquet operator in Eq. (4) equivalently as describing a nonreciprocal KHM, or NRKHM, in short. Interestingly, Anderson transitions in quasiperiodic KHM (with irrational α) was also investigated in early studies [77–79]. While non-Hermitian effects on the

spectral and localization transitions in the KHM have yet to be revealed. Throughout this paper, we will choose α to be the inverse golden ratio, i.e., $\alpha = \frac{\sqrt{5}-1}{2}$, to endow the lattice with spatial quasiperiodicity. We will also perform all our numerical studies of the $\hat{U}$ in Eq. (4) under the PBC, such that the possible influence non-Hermitian skin effect is absent.

The NRKHM considered here is closely related to experimentally realizable physical systems. Recently, a quasiperiodic KHM was realized by applying apodized Floquet engineering techniques to ultracold ^{84}Sr atoms [83]. In the Hermitian limit ($\gamma = 0$), the Floquet operator of our model is exactly equivalent to the one realized in Ref. [83]. The direct realization of finite nonreciprocal hopping is challenging for cold-atom setups. Recently, techniques to effectively engineer nonreciprocal hopping for cold atoms have been considered in both theory and experiments by introducing atomic losses [53,84–86]. Cold-atom systems are thus good candidates to realize our model and probe its physical properties in near-term experiments. On the other hand, $\mathcal{PT}$ and localization transitions in a temporally driven (Floquet) dissipative quasicrystal were recently observed [58]. The experiment there is implemented by photonic quantum walks in coupled optical fiber loops. The model realized in Ref. [58] may be viewed as a dynamical variant of the NRHM, which contains two key elements for the realization of our model, i.e., the piecewise periodic quench and the nonreciprocal hopping. Meanwhile, only a transition between localized and delocalized phases accompanied by the breaking of $\mathcal{PT}$ symmetry is observed in Ref. [58] due to the short-range nature of the realized hopping amplitudes. By implementing long-range steps to the walker in modified versions of the system in Ref. [58], the evolution operator for the hopping part of our model may be realized. Therefore, photonic quantum walks can also serve as a candidate to realize our system and detect the multiple $\mathcal{PT}$ and reentrant localization transitions there.

III. METHOD

In this section, we outline essential tools that will be employed to characterize various non-Hermitian Floquet quasicrystalline phases and the transitions among them in the NRKHM.

The spectral and state properties of the NRKHM can be addressed by solving the eigenvalue equation $\hat{U}|\psi_j\rangle = e^{-iE_j}|\psi_j\rangle$ for the Floquet operator $\hat{U}$ in Eq. (4). Here E_j is the quasienergy of the jth right eigenvector $|\psi_j\rangle$, which can take complex values as $\hat{U}$ is nonunitary. For a lattice of length L, there are L such eigenstates indexed by $j = 1, ..., L$. To check whether $\mathcal{PT}$-breaking transitions could happen, we consider the maximal imaginary parts of E and the density of states (DOS) ρ with nonreal quasienergies [87–89], which are defined as

$$\max|\mathrm{Im}E| = \max_{j\in\{1,...,L\}}(|\mathrm{Im}E_j|), \tag{5}$$

$$\rho = N(\mathrm{Im}E \neq 0)/L. \tag{6}$$

Here $N(\mathrm{Im}E \neq 0)$ means the number of states whose quasienergies have nonvanishing imaginary parts. It is clear that once the $\max|\mathrm{Im}E|$ switches from zero to a finite value, eigenstates with complex quasienergies would appear in the Floquet spectrum. A $\mathcal{PT}$-breaking transition then happens in the NRKHM, which is further accompanied by the deviation of ρ from zero. Moreover, we would have $\rho \simeq 1$ when almost all eigenstates of $\hat{U}$ possess nonreal quasienergies. We can thus use $\max|\mathrm{Im}E|$ and ρ to distinguish phases with different spectral nature.

The localization properties of Floquet eigenstates in the NRKHM can be characterized by their level-spacing statistics and inverse participation ratios (IPRs) [87–89]. If the set of quasienergies $\mathcal{E} = \{E_j|j = 1, ..., L\}$ has been sorted by their real parts, we can identify the real level-spacing between the jth and the $(j-1)$th element in the set $\mathcal{E}$ as $\epsilon_j = \mathrm{Re}E_j - \mathrm{Re}E_{j-1}$. The ratio between adjacent level spacings can be defined as $g_j = \min(\epsilon_j, \epsilon_{j+1})/\max(\epsilon_j, \epsilon_{j+1})$ for $j = 2, ..., L-1$, where $\min(\epsilon, \epsilon')$ and $\max(\epsilon, \epsilon')$ yield the minimum and maximum of ϵ and ϵ'. The statistical feature of adjacent gap ratios (AGRs) g_j can be determined by the average of AGRs over all states [90–94], i.e.,

$$\bar{g} = \frac{1}{L}\sum_j g_j. \tag{7}$$

If all bulk states are extended in the thermodynamic limit $L \to \infty$, we would have $\bar{g} \to 0$. For a phase in which all bulk states are localized, $\bar{g}$ would instead approach a finite constant $\bar{g}_{\max} > 0$. If there is a critical region in which extended and localized eigenstates coexist and are separated by a mobility edge, $\bar{g}$ is nonuniversal and takes values in a range $\bar{g} \in (0, \bar{g}_{\max})$. The behavior of $\bar{g}$ can thus be employed to distinguish phases with different localization natures in the NRKHM. The IPR is another direct measure of the state profiles in the system. For a given normalized right eigenvector $|\psi_j\rangle = \sum_{n=1}^{L}\psi_n^j|n\rangle$ of $\hat{U}$ with quasienergy E_j in the lattice basis, we define its IPR as $\mathrm{IPR}_j = \sum_{n=1}^{L}|\psi_n^j|^4$. A conjugate quantity, called the normalized participation ratio (NPR) can be constructed for the state $|\psi_j\rangle$ as $\mathrm{NPR}_j = (\sum_{n=1}^{L}|\psi_n^j|^4)^{-1}/L$. If $|\psi_j\rangle$ happens to be a localized state (an extended state), we would have $\mathrm{IPR}_j \to \lambda_j$ ($\mathrm{IPR}_j \to 0$) and $\mathrm{NPR}_j \to 0$ ($\mathrm{NPR}_j \to 1$), where the Lyapunov exponent λ_j can be a function of the quasienergy E_j. The global localization property of the system can then be inspected by averaging the IPRs and NPRs over all bulk states, yielding

$$\mathrm{IPR}_{\mathrm{ave}} = \frac{1}{L}\sum_{j=1}^{L}\mathrm{IPR}_j, \tag{8}$$

$$\mathrm{NPR}_{\mathrm{ave}} = \frac{1}{L}\sum_{j=1}^{L}\mathrm{NPR}_j. \tag{9}$$

Moreover, we introduce the minimum/maximum of IPRs and an extra quantity ζ to capture the transitions between different phases in the system and the presence of critical phase with mobility edge. These quantities are explicitly defined as

$$\mathrm{IPR}_{\max} = \max_{j\in\{1,...,L\}}(\mathrm{IPR}_j), \tag{10}$$

$$\mathrm{IPR}_{\min} = \min_{j\in\{1,...,L\}}(\mathrm{IPR}_j), \tag{11}$$

$$\zeta = \log_{10}(\mathrm{IPR}_{\mathrm{ave}}\cdot\mathrm{NPR}_{\mathrm{ave}}). \tag{12}$$

It is clear that once the first (last) localized (extended) bulk state appears (vanishes) in the system, the $\mathrm{IPR}_{\max}$ ($\mathrm{IPR}_{\min}$) will be found to deviate from zero in the limit $L \to \infty$. Moreover, the value of ζ can be finite only when $\mathrm{IPR}_{\mathrm{ave}} \cdot \mathrm{NPR}_{\mathrm{ave}} \neq 0$, which means that finite amounts of extended and localized states could survive together in the system. Therefore, the NRKHM described by $\hat{U}$ resides in the extended, localized, or critical mobility edge phase if $\mathrm{IPR}_{\max} \to 0$, $\mathrm{IPR}_{\min} > 0$, or ζ being finite in the thermodynamic limit, respectively.

To probe the transport nature of different phases in the NRKHM, we consider the dynamics of wave packets [76]. The stroboscopic evolution of an initial state $|\psi(0)\rangle$ over ℓ driving periods yields the state $|\tilde{\psi}(t=\ell T)\rangle = \hat{U}^{\ell}|\psi(0)\rangle$, which is not normalized in the lattice representation for a nonunitary $\hat{U}$. Using the normalization convention of right eigenvectors, the normalized state after an evolution over $t = \ell T$ driving periods takes the form $|\psi(t)\rangle = |\tilde{\psi}(t)\rangle/\sqrt{\langle\tilde{\psi}(t)|\tilde{\psi}(t)\rangle}$. Expanding $|\psi(t)\rangle$ in the lattice basis produces the probability amplitude $\psi_n(t) = \langle n|\psi(t)\rangle$ of the evolved state at different locations of the lattice, i.e., $|\psi(t)\rangle = \sum_n \psi_n(t)|n\rangle$. To characterize the stroboscopic dynamics of the wave packet, we investigate the time dependence of its center $x(t)$, standard deviation $x_{\mathrm{sd}}(t)$, and averaged spreading speed $v(t)$ in the lattice, which are defined as

$$x(t) = \sum_n n|\psi_n(t)|^2, \tag{13}$$

$$x_{\mathrm{sd}}(t) = \sqrt{\sum_n n^2|\psi_n(t)|^2 - x^2(t)}, \tag{14}$$

$$v(t) = \frac{1}{t}\sqrt{\sum_n n^2|\psi_n(t)|^2}. \tag{15}$$

Here $t = \ell T$ refers to the stroboscopic time with $\ell \in \mathbb{Z}$. For a localized initial state in the lattice, we expect $x(t)$ [$x_{\mathrm{sd}}(t)$] to stay close to its initial value in the localized phase, $x(t) \propto t$ [$x_{\mathrm{sd}}(t) \propto \sqrt{t}$] in the extended phase due to the nonreciprocal hopping in the system, and $x(t)$ [$x_{\mathrm{sd}}(t)$] to show an intervening behavior in the critical phase with mobility edge. For the same initial state and over a long evolution time ($\ell \gg 1$), the average speed $v(t)$ should tend to vanish in the localized phase, become finite in the intermediate phase with a mobility edge due to the presence of hopping asymmetry, and taking maximal values in the extended phase. We can thus employ $x(t)$, $x_{\mathrm{sd}}(t)$, and $v(t)$ to dynamically distinguish phases with different transport properties in the NRKHM.

IV. RESULTS

We are now ready to uncover the spectral and localization nature of the quasiperiodic NRKHM with the help of the tools introduced in the last section. In Fig. 2, we present the maximal imaginary parts of E [Eq. (5)], the DOS with nonreal quasienergies [Eq. (6)], the minimum of IPRs [Eq. (11)], and the spreading speed of an initially localized excitation [Eq. (15)] versus the on-site potential V for a typical set of system parameters. Interestingly, we observe complex and highly monotonous behaviors for all these quantities, which are drastically different from the cases observed in the nondriven [75,76] or high-frequency

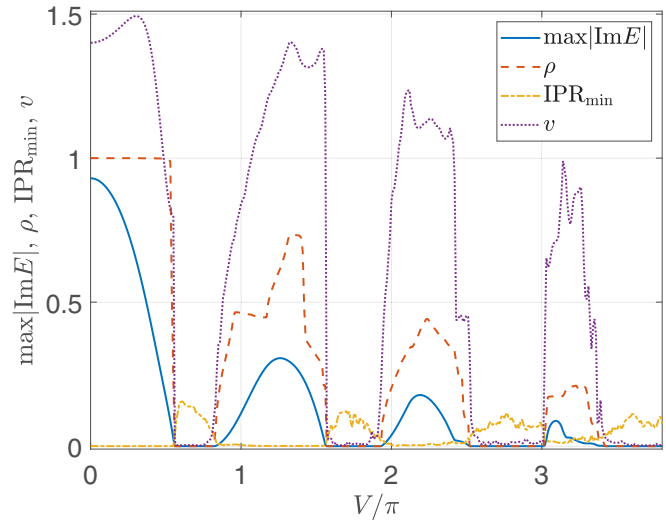

FIG. 2. Maximal imaginary parts of quasienergy (blue solid line), DOS with nonreal quasienergies (red dashed line), minimum of IPRs (yellow dash-dotted line), and averaged spreading velocity of a wave packet (purple dotted line) versus the on-site potential amplitude V under the PBC. Other system parameters are $(J, \gamma) = (\pi/6, 0.8)$. The lattice size is $L = 4181$. The initial state in the calculation of $v = v(t)$ is chosen to be $|\psi(0)\rangle = \sum_n \delta_{n0}|n\rangle$. The average in Eq. (15) is taken over 1000 driving periods.

driven [59] NRHM. Specially, the $\mathcal{PT}$ symmetry is broken and the Floquet spectrum of the system is complex at $V = 0$ (i.e., the clean lattice limit). With the increase of V, the quasienergy spectrum could first undergo a $\mathcal{PT}$-restoring transition from complex to real. But later it becomes complex again after a $\mathcal{PT}$-breaking transition with the further increase of V. In the second complex-spectrum phase, the ratio of states with nonreal quasienergies ρ is finite but smaller than 1, which means that states with real and complex quasienergies coexist in this phase. With the further increase of V, the NRKHM encounters a sequence of $\mathcal{PT}$-restoring and $\mathcal{PT}$-breaking transitions, while its quasienergy spectrum alternates between purely real and partially complex in different parameter regions. More interestingly, the $\mathrm{IPR}_{\min}$ is pinned to zero in the phases with complex quasienergies and deviates from zero whenever the spectra become real. This suggests that all eigenstates in real-spectrum phases of the NRKHM are localized, whereas extended eigenstates emerge whenever nonreal quasienergies appear in the Floquet spectrum. The connection between the realness of the Floquet spectrum and the localization nature of states is further confirmed by investigating the spreading of a localized initial wave packet, whose average speed is finite in the regions with $\max|\mathrm{Im}E| > 0$, $\mathrm{IPR}_{\min} \simeq 0$ but vanishes in the domains with $\max|\mathrm{Im}E| = 0$, $\mathrm{IPR}_{\min} > 0$, yielding the phenomenon of dynamical localization in real-spectrum phases of the NRKHM.

To further clarify the relationship between the structure of spectrum and the states' localization property in the NRKHM, we pick out a set of typical parameters from Fig. 2 and show the corresponding quasienergy spectra on the complex plane together with the IPRs of all Floquet eigenstates in Fig. 3. With a weak quasiperiodic potential ($V = 0.2\pi$), all

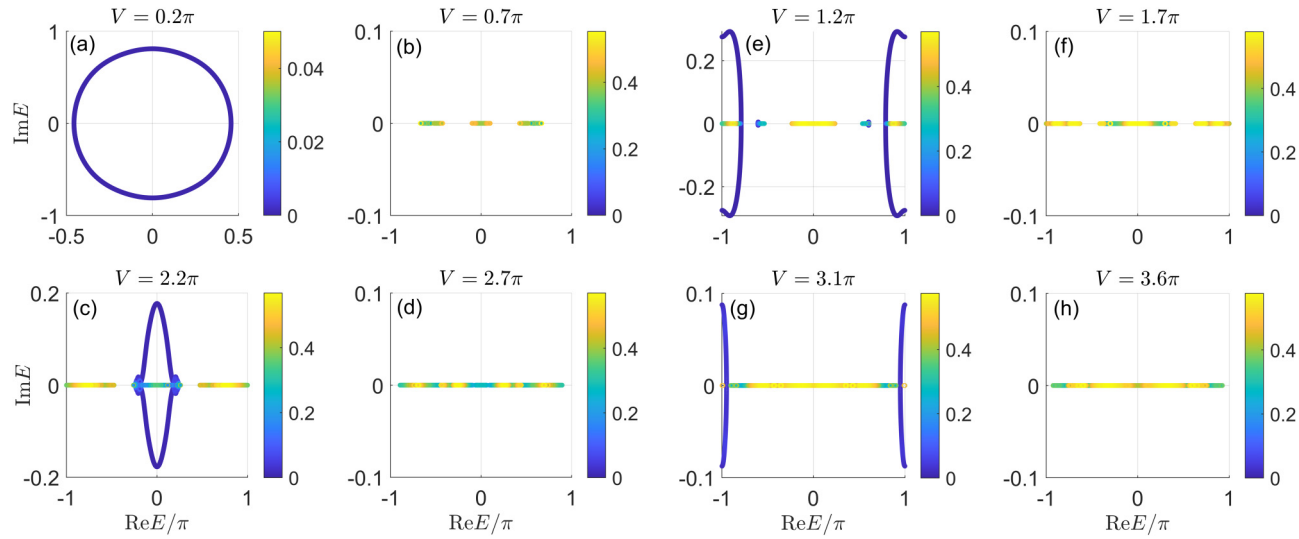

FIG. 3. Floquet spectrum $E = \mathrm{Re}E + i\mathrm{Im}E$ on the complex plane (in circles) and IPRs (in color scale) of the NRKHM under PBC for eight typical cases. The amplitude V of on-site quasiperiodic potential is shown in the caption of each figure panel. Other system parameters are set as $(J, \gamma) = (\pi/6, 0.8)$. The length of lattice is chosen to be $L = 4181$ for all panels.

states are found to be extended (IPR $\simeq 0$) and taking nonreal quasienergies with the hopping asymmetry $\gamma \neq 0$, as shown in Fig. 3(a). For parameters chosen within the real-spectrum phases of Fig. 2 ($V = 0.7\pi, 1.7\pi, 2.7\pi, 3.6\pi$), we instead observe localization for all Floquet eigenstates (IPR > 0) as shown in Figs. 3(b), 3(d), 3(f), and 3(h). For parameters taken in the second ($V = 1.2\pi$), third ($V = 2.2\pi$), and fourth ($V = 3.1\pi$) mixed-spectrum phases of Fig. 2, we find the coexistence of real and nonreal quasienergies in different regions of the spectrum. Moreover, eigenstates with real (nonreal) quasienergies are found to be localized (extended) in all the three cases, as shown in Figs. 3(c), 3(e), and 3(g). The mixed-spectrum phases appearing at larger V thus coincide with the critical phases of NRKHM, in which localized real-quasienergy eigenstates and extended nonreal-quasienergy eigenstates are separated by mobility edges on the complex plane. Therefore, as a result of the competition among driving, non-Hermiticity and disorder, the quasiperiodic NRKHM possesses at least three distinct phases, i.e., an extended phase with a purely complex spectrum, a localized phase with a real spectrum, and a critical phase wherein states with real and nonreal quasienergies coexist and are separated by mobility edges.

To consolidate the presence of the three possible phases in the thermodynamic limit, we show in Fig. 4 the scaling of IPRs versus the lattice size L for the eight representative cases of Fig. 3 under the PBC. As expected, we find that the $\mathrm{IPR}_{\mathrm{max}}$ [Eq. (10)], $\mathrm{IPR}_{\mathrm{ave}}$ [Eq. (8)], and $\mathrm{IPR}_{\mathrm{min}}$ [Eq. (11)] are all $\propto L^{-1}$ with the increase of L in Fig. 4(a), implying that all eigenstates are extended in the phase with purely complex spectrum. Comparatively, for parameters taken in the real-spectrum phases, we find almost no changes in $\mathrm{IPR}_{\mathrm{max}}$, $\mathrm{IPR}_{\mathrm{ave}}$ and $\mathrm{IPR}_{\mathrm{min}}$ with the increase of L as shown in Figs. 4(b), 4(d), 4(f), and 4(h), meaning that all states in these cases are localized. For parameters taken in the mixed-spectrum phases, the $\mathrm{IPR}_{\mathrm{max}}$ is found to be independent of L, whereas the $\mathrm{IPR}_{\mathrm{min}}$ is inversely proportional to L as shown in Figs. 4(c), 4(e), and 4(g), verifying that localized and extended states coexist in the system in these cases. The real-spectrum localized, complex-spectrum extended and mixed-spectrum critical mobility edge phases of the NRKHM are thus expected to survive in the thermodynamic limit $L \to \infty$.

To acquire a more complete understanding of the phases and transitions in the NRKHM, we present the DOS [Eq. (6)], the averaged AGRs [Eq. (7)], the minimum of IPRs [Eq. (11)], and the measure of critical mobility edge phase ζ [Eq. (12)] versus the amount of hopping asymmetry γ and the on-site potential V in Fig. 5. The consistency of the results among the four panels of Fig. 5 clearly suggests the presence of an extended phase (with $\rho \simeq 1$, $\bar{g} \simeq 0$, $\mathrm{IPR}_{\mathrm{min}} \simeq 0$, and $\zeta \to -\infty$), a localized phase (with $\rho \simeq 0$, $\bar{g} \simeq 0.6$, $\mathrm{IPR}_{\mathrm{min}} > 0$, and $\zeta \to -\infty$) and a critical mobility edge phase (with $0 < \rho < 1$, $0 \lesssim \bar{g} \lesssim 0.6$, $\mathrm{IPR}_{\mathrm{min}} > 0$, and ζ finite) in the NRKHM. When the non-Hermitian parameter γ is small, the change of the quasiperiodic potential amplitude V can only cause a transition of the system from a complex-spectrum extended phase to a real-spectrum localized phase, which is similar to what happens in the nondriven NRHM [75,76]. When the hopping asymmetry γ is large enough, non-Hermitian effects are dominant. In this region, we only find the transition from a complex-spectrum extended phase to a mixed-spectrum critical phase in Fig. 5. This observation suggests that real-quasienergy extended states could persist in the NRKHM over a broad range of quasiperiodic potential amplitudes V at strong non-Hermiticity. In the intermediate range of γ, however, we find reentrant spectral and localization transitions between real-spectrum localized and mixed-spectrum critical phases with the increase of V. This observation demonstrates unambiguously that the rich phase and transition patterns in the NRKHM indeed originate from the interplay among three nontrivial effects when they are comparable, i.e., the non-Hermiticity, Floquet driving, and spatial quasiperiodicity. The original phase diagram of the NRHM [75,76] gets most strongly modified when both the hopping nonreciprocity and the driving field reach sufficient strengths.

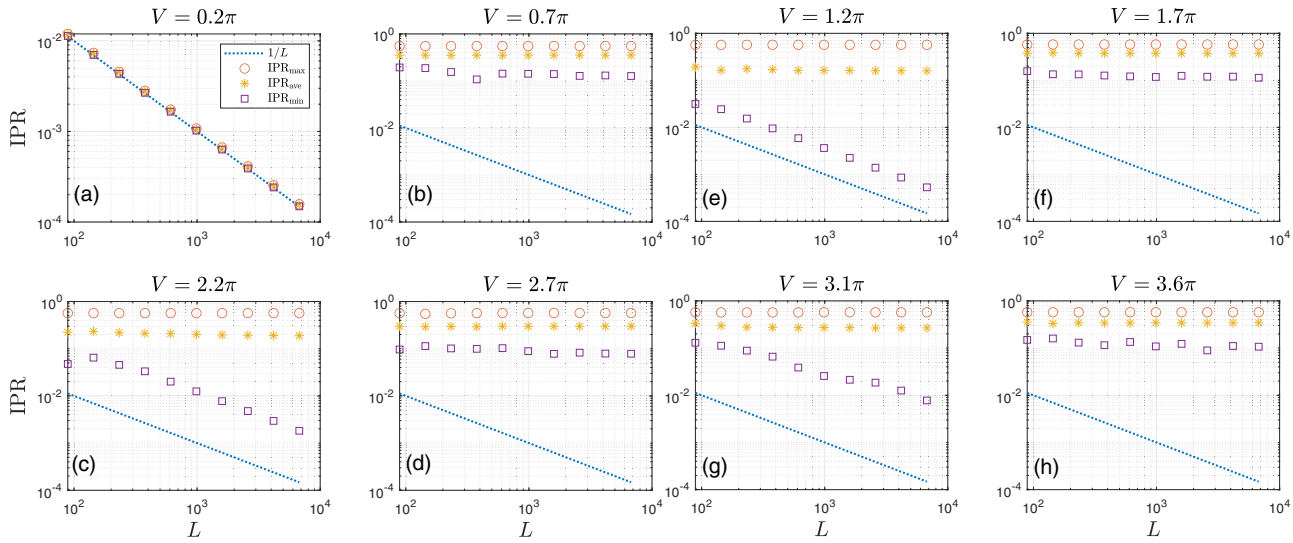

FIG. 4. Scaling of the IPRs of right eigenvectors versus system size L under the PBC, shown in log-log plot. In all panels, the dotted lines, circles, stars, and squares denote the values of $1/L$, $\mathrm{IPR_{max}}$, $\mathrm{IPR_{ave}}$ and $\mathrm{IPR_{min}}$ at different lattice sizes L for $L = 89, 144, 233, 377, 610, 987, 1597, 2584, 4181, 6765$. The amplitude V of the on-site potential is given in the caption of each figure panel. Other system parameters are set as $(J, \gamma) = (\pi/6, 0.8)$.

The presence of extended, localized, and critical phases in the NRKHM has immediate dynamical implications, which could help us to detect and differentiate them in experiments. To achieve this goal, we consider the dynamics of a single-site excitation in the lattice under the PBC, which is described by the theory introduced in Sec. III. The spatial distribution of probability amplitude $|\psi_n(t)| = |\langle n|\psi(t)\rangle|$ of at different stroboscopic times $t = \ell T$ ($\ell \in \mathbb{Z}$) in the system are shown in Fig. 6 for the eight exemplary cases reported in previous spectrum and localization studies. In Fig. 6(a), the system is in an extended phase and the wave packet shows a unidirectional transport with a limited width of spreading. The former is due to the asymmetric hopping of the lattice, i.e., tunneling from the right to left lattice sites is stronger then the opposite for a positive γ. In Figs. 6(b), 6(d), 6(f), and 6(h), the system is set in real-spectrum localized phases and the excitation tends to be localized around its initial position up to small oscillations. All states in the system in these cases are thus not only spatially but also dynamically localized. For systems prepared in the critical mobility edge phase, the initial excitation is still found to be able to propagate unidirectionally with a well-localized profile during the evolution, as shown in Figs. 6(c), 6(e), and 6(g). However, two differences are observed compared with the case shown in Fig. 6(a). First, the distance between the final and initial locations of the wave packet in the critical phase is smaller then that in the extended phase. This means that the excitation has a smaller propagation speed on average when evolving in the critical phase, which is due to the presence of localized Floquet eigenmodes that could hinder its transport there. Second, the location of the wave packet shows a smooth and linear growth with time in the extended phase, whereas in the critical phase, the location of excitation could be pinned in space for some time during the evolution, and then grows through tunneling to farther sites within a relatively short time window, which is a unique phenomenon in non-Hermitian transport.

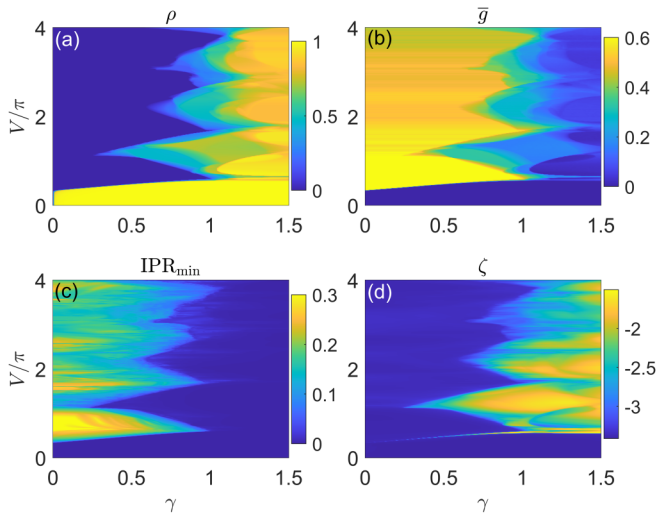

FIG. 5. The DOSs ρ, averaged AGRs $\bar{g}$, minimum of IPRs $\mathrm{IPR_{min}}$ and probe of critical mobility edge phase ζ versus the hopping asymmetry parameter γ and on-site potential amplitude V under the PBC. The uniform part of hopping amplitude is $J = \pi/6$ and the length of the lattice is $L = 2584$ for all calculations.

For completeness, we present the time dependence of the center [Eq. (13)] and standard deviation [Eq. (14)] of the same initial excitation for the eight parameter sets in Fig. 7. The results confirm our observations of the wave-packet dynamics for the corresponding cases in Fig. 6. Put together, the markedly different dynamical behaviors of wave packets in distinct parameter regions of the NRKHM could indeed provide us with a means to probe and distinguish the extended, localized, and critical phases therein.

V. DISCUSSION

We now discuss more about the physical origin of the rich phase patterns and multiple reentrant transitions in the

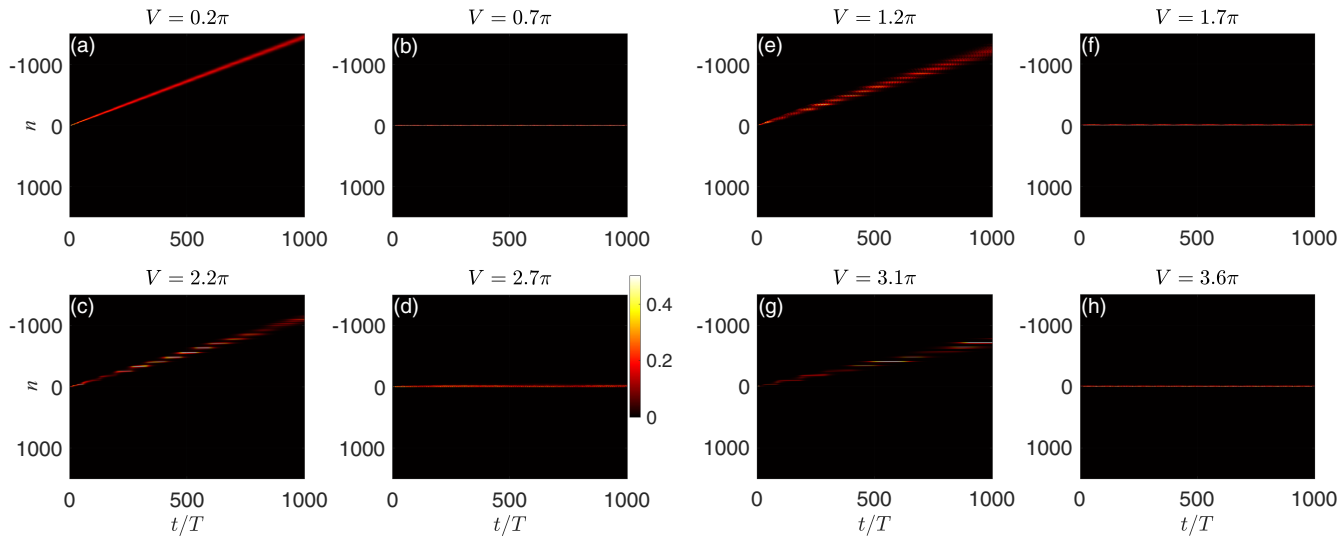

FIG. 6. Propagation of an initially localized wave packet $|\psi(0)\rangle = \sum_n \delta_{n0}|n\rangle$ in the NRKHM under the PBC. The color scale denotes the absolute amplitude of the evolving state in the lattice at the time $t = \ell T$ for $\ell = 1, 2, ..., 999, 1000$. All panels share the same color bar. The values of on-site potential amplitude V are given in corresponding figure captions. Other system parameters are $(J, \gamma) = (\pi/6, 0.8)$. The length of the lattice is $L = 4181$ and the lattice site index (vertical axis) takes values from $n = -2090$ to $n = 2090$.

NRKHM. In general, $\mathcal{PT}$ transitions in nNHQCs could appear due to the competition between Hermitian and non-Hermitian effects. Without Floquet driving fields, the impacts of Hermitian terms (the on-site potential in our case) or non-Hermitian terms (the asymmetric hopping in our case) usually change monotonically with the increase of their control parameters (V for the Hermitian and γ for the non-Hermitian term in our model). In this case, there is only a single $\mathcal{PT}$ transition when the strengths of the control parameters of Hermitian (or non-Hermitian) terms dominate (exceptions exist in systems with dimerized lattice structures [89]). With Floquet driving fields, the impacts of Hermitian and non-Hermitian terms may not change monotonically with the increase of their control parameters. Their competitions in the presence of this nonmonotonicity could then result in the multiple $\mathcal{PT}$ and reentrant localization transitions in NHQCs.

In our system, the Floquet operator in Eq. (4) can be equivalently written as $\hat{U} = e^{-i\hat{H}_2 T/\hbar} e^{-i\hat{H}_1 T/\hbar} = e^{-i\hat{H}_{\rm eff} T/\hbar}$, where $\hat{H}_1 = \hat{K}T_1/T$ and $\hat{H}_2 = \hat{V}T_2/T$ represent rescaled hopping and on-site potential terms in the quenched Hamiltonian. According to the Baker-Campbell-Hausdorff formula [95], the effective Hamiltonian $\hat{H}_{\rm eff}$ can be expanded into a series as

$$\hat{H}_{\rm eff} = \hat{H}_1 + \hat{H}_2 + \frac{iT}{2}[\hat{H}_1, \hat{H}_2] + \frac{T^2}{12\hbar^2}[\hat{H}_2 - \hat{H}_1, [\hat{H}_1, \hat{H}_2]] + \cdots \tag{16}$$

The combination of the first two terms on the right-hand-side (RHS) of Eq. (16) just yields the static NRHM, which does not hold any signatures of critical mobility edge phases [75,76]. However, the third, fourth, and higher order terms in the expansion on the RHS of Eq. (16) contain commutators

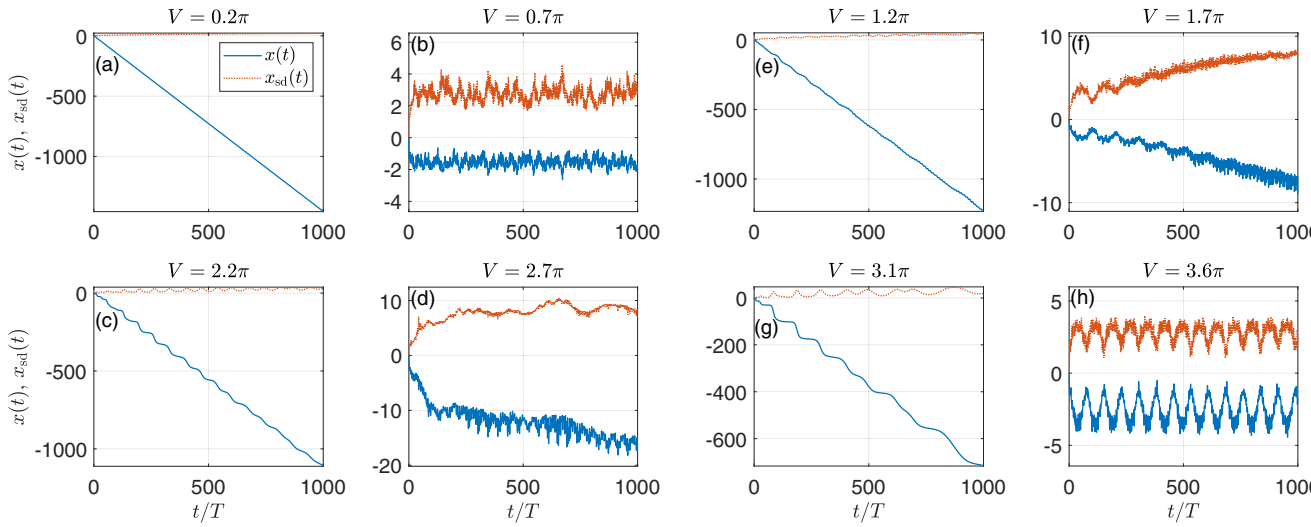

FIG. 7. Time dependence of the mean position $x(t)$ and standard deviation $x_{\rm sd}(t)$ of a localized initial excitation $|\psi(0)\rangle = \sum_n \delta_{n0}|n\rangle$ at the center of the NRKHM under the PBC. The lattice size and system parameters are the same as those used in Fig. 6.

between the on-site potential and nearest-neighbor hopping terms, which can yield asymmetric hoppings beyond nearest-neighbor sites in the driven lattice. With quasiperiodic disorder, these long-range hopping terms made possible by the driving field are the usual origin of mobility edges in both tight-binding lattices and continuous models [96–98]. In Appendix A, we give a brief discussion of the system at the level of $\hat{H}_{\text{eff}}$ in Eq. (16) by truncating the series at the order T^2. The results indeed provide evidence for the presence of reentrant localization transitions in the NRKHM. Second, on each lattice site, the magnitude of $\hat{V}$ in $\hat{H}_2$ is defined modulus 2π. Therefore, the contribution of each on-site term $\mathsf{V}_n = VT_2\cos(2\pi\alpha n)/\hbar$ to the diagonal elements of $e^{-i\hat{H}_2 T/\hbar}$ and thus to $\hat{U}$ is 2π periodic. This fact, in combination with other quasiperiodic terms generated by the commutators in Eq. (16) allow the effective strength of correlated disorder to depend on V in a nonmonotonic and oscillatory manner. Such a quasiperiodic V dependence, which is also enabled by the driving field, finally causes the reentrant transitions between real-spectrum localized phases and mixed-spectrum critical phases in the NRKHM. Notably, the range of on-site potential V considered in our study clearly includes cases of strong and resonant drivings. Our findings thus go beyond previous results focusing on high-frequency modulation schemes [59,99].

Specially, in Ref. [59], a harmonic driving force of the form $\sum_n nK\cos(\omega t)$ was applied to NHQCs and the high-frequency limit was taken. The hopping amplitude J is dressed by the Floquet field into the form $J_{\text{eff}} = J\mathcal{J}_0(K/\omega)$, with K (ω) the driving amplitude (frequency) and $\mathcal{J}_0$ the Bessel function. Due to the nonmonotonic dependence of $\mathcal{J}_0(K/\omega)$ on K/ω, J_{eff} can also change with the driving parameter K/ω in a nonmonotonous way, and multiple $\mathcal{PT}$ transitions could appear. Compared with the present work, a main difference is that in Ref. [59], the possible number of NHQC phases is not modified by the driving. The driving field mainly achieves the control of the transition boundary between different phases. However, in the present paper, the strong and near-resonant driving field creates multiple critical phases with mobility edges, which are absent when the driving field is switched off or the high-frequency limit is taken. The driving field further induces transitions between the newly formed critical phases and other phases with different localization nature, which are also absent in the nondriven setup. Therefore, the driving field in the present paper plays a more nonperturbative and nontrivial role compared with what it did in Ref. [59]. Besides, the driving is introduced here as time-periodic quenches, whose effect may be viewed as the superposition of many harmonic drives with different frequencies and amplitudes [100]. The hybrid nature of the drive and the long-range coupling it induced allow us to have richer patterns of non-Hermitian Floquet quasicrystal phases in the NRKHM.

VI. SUMMARY

In this paper, we found that the interplay among time-periodic driving, hopping nonreciprocity, and correlated disorder could induce critical phases with mobility edges, multiple $\mathcal{PT}$ transitions, and reentrant localization transitions in 1D lattices. The corresponding non-Hermitian Floquet quasicrystals possess rich phase patterns with a distinct spectral and transport nature, which are characterized by the level-spacing statistics, IPRs, and wave-packet dynamics. The reentrant transitions among localized and critical phases in the system physically originate from the 2π periodicity in the amplitude of the periodically modulated on-site potential and the effective long-range hopping generated by high-order commutators between kinetic and potential energy terms. Our results thus establish in aperiodic systems a unique class of non-Hermitian Floquet matter, which holds rich and highly tunable spectral, dynamical, and localization properties.

Two implications of our results deserve to be emphasized. First, the multiple $\mathcal{PT}$ transitions and reentrant localization transitions in our system emerge only when $\gamma \neq 0$ and the quasiperiodic quench strength V is relatively large. These transitions are thus induced by the strong interplay between Floquet driving fields and non-Hermitian effects in a disordered system. To the best of our knowledge, the multiple and reentrant transitions originating from the corporation between these two nonequilibrium knobs were not revealed in previous studies of NHQCs or Floquet states of matter, or largely overlooked in related work [58,99,101]. Second, the multiple lobes appearing at finite hopping nonreciprocity and quasiperiodic quench potential contain both extended and localized states. These lobes represent critical phases with quasienergy-dependent mobility edges (see Fig. 4) in non-Hermitian Floquet quasicrystals, instead of describing localized regimes. Notably, these critical phases are absent when either the driving field or the non-Hermitian effect is switched off. Therefore, the emergence of these critical phases is a unique outcome of the nontrivial collaboration among driving, disorder, and non-Hermitian effects in our system. This discovery goes beyond the previous finding [59], in which high-frequency drivings only modulate the hopping amplitude and lead to the deformation of the phase diagram without changing the number of possible phases that could appear. Our discovery thus uncovered that exceeding the high-frequency regime, the driving field could create unique NHQCs beyond the underlying nondriven system.

In future work, it would be interesting to consider Floquet quasicrystals with lattice dimerization [102–104] (one such example is treated briefly in Appendix B), in higher spatial dimensions, and in systems with other non-Hermitian effects like on-site gain and loss. The impact of interactions and the possible appearance of non-Hermitian Floquet many-body localized phases in quasiperiodic systems also deserve more thorough explorations.

ACKNOWLEDGMENTS

L.Z. is supported by the National Natural Science Foundation of China (Grant No. 11905211), the Young Talents Project at Ocean University of China (Grant No. 861801013196), and the Applied Research Project of Postdoctoral Fellows in Qingdao (Grant No. 861905040009).

APPENDIX A: PHASE TRANSITIONS DESCRIBED BY $\hat{H}_{\text{eff}}$

In this Appendix, we briefly discuss the transitions in the system described by the $\hat{H}_{\text{eff}}$ in Eq. (16). We truncate the

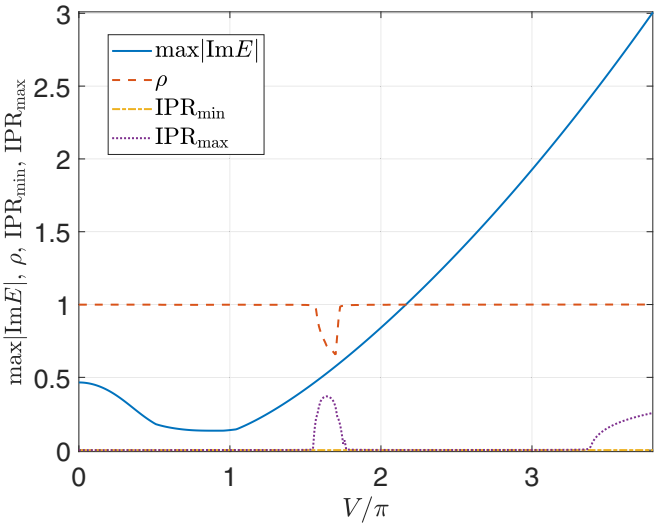

FIG. 8. Maximal imaginary parts of quasienergy (blue solid line), DOS with nonreal quasienergies (red dashed line), minimum and maximum of IPRs (yellow dash-dotted and purple dotted lines) of the $\hat{H}_{\text{eff}}$ versus the on-site potential amplitude V under the PBC. Other system parameters are $(J, \gamma) = (\pi/6, 0.8)$. The lattice size is $L = 4181$

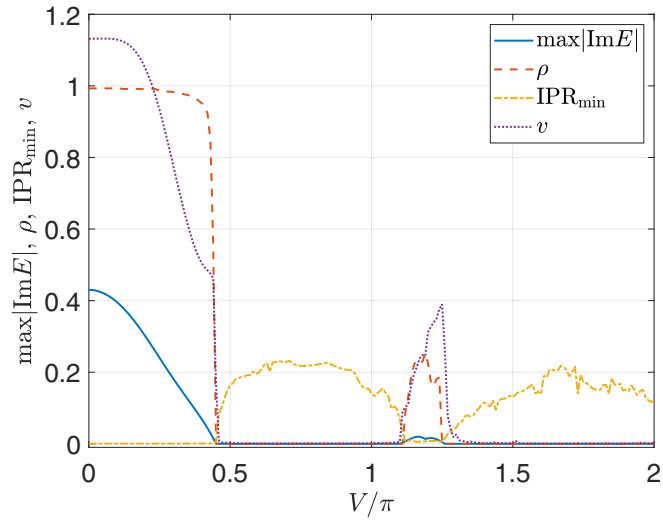

FIG. 9. Maximal imaginary parts of quasienergy (blue solid line), DOS with nonreal quasienergies (red dashed line), minimum of IPRs (yellow dash-dotted line) and averaged spreading velocity a of wave packet (purple dotted line) of the dimerized NRKHM versus the on-site potential amplitude V under the PBC. Other system parameters are $(J, \gamma) = (\pi/6, 0.8)$. The lattice size is $L = 2584$. The initial state in the calculation of $v = v(t)$ is chosen to be $|\psi(0)\rangle = \sum_n \delta_{n0}|n\rangle$. The average in Eq. (15) is taken over 1000 driving periods.

series at the order T^2, i.e., to include all the terms explicitly shown in Eq. (16). In Fig. 8, we present the properties of spectrum and IPR of the $\hat{H}_{\text{eff}}$. The results demonstrate the presence of reentrant transitions between extended and critical mobility edge phases in the system at the level of $\hat{H}_{\text{eff}}$. The is consistent with our argument in the main text that the reentrant localization transitions originate from long-range couplings induced by the Floquet driving. However, no $\mathcal{PT}$ transitions and localized phases are observed for the considered domain of superlattice potential V. This is expected, as the driving frequency $\Omega = 2\pi/T$ is equal to π in our calculation, which is comparable with other parameters J and V of the system. In such a storng and near-resonant driving regime, higher order terms in $\hat{H}_{\text{eff}}$ may also have important contributions, and one should not expect to capture the whole physics at the level of $\hat{H}_{\text{eff}}$ by truncating the series in Eq. (16) at a finite order. The problem is essentially nonperturbative. Moreover, the 2π periodicity of $\hat{U}$ in V_n is also lost at the level of $\hat{H}_{\text{eff}}$, and the second part of our argument in Sec. V does not work in this case. Therefore, we emphasize that a full numerical treatment of the Floquet operator $\hat{U}$ is needed to capture the complete physics of quasienergy spectrum and localization transitions in the NRKHM (and also, in general, non-Hermitian Floquet quasicrystals) in strong and near-resonant driving regimes.

APPENDIX B: PHASE TRANSITIONS IN A DIMERIZED NRKHM

In this Appendix, we briefly consider the $\mathcal{PT}$ and localization transitions in a dimerized variant of the NRKHM. Lattice dimerization may be introduced to the on-site potential or hopping amplitude. For simplicity, we consider a dimerized hopping model by replacing $\hat{K}$ in Eq. (1) with

$$\hat{K}' = J\sum_n (e^{\gamma}|2n-1\rangle\langle 2n| + e^{-\gamma}|2n\rangle\langle 2n-1|) + J\sum_n (|2n\rangle\langle 2n+1| + \text{H.c.}). \tag{B1}$$

Following the same quench protocol as given by Eq. (3) in the main text, the resulting Floquet operator of the system reads $\hat{U}' = e^{-i\hat{V}T_2/\hbar}e^{-i\hat{K}'T_1/\hbar}$. In Fig. 9, we present the $\mathcal{PT}$ and localization transitions of this dimerized NRKHM versus the strength of on-site potential V with $T_1 = T_2 = 1$. The Floquet spectrum, IPR and wave-packet velocity are computed by the method sketched in Sec. II. We find again multiple $\mathcal{PT}$ transitions, critical phases with mobility edges, and reentrant localization transitions in this dimerized NRKHM. Nevertheless, the transition points and ranges of the critical phase are different from the original model due to the effect of dimerized hopping. Meanwhile, lattice dimerization may also induce other interesting physics in non-Hermitian Floquet quasicrystals, such as richer phase patterns, more localization transitions, and new topological properties. We leave a thorough investigation of this issue to potential future studies.

[1] T. Kitagawa, Topological phenomena in quantum walks: Elementary introduction to the physics of topological phases, Quantum Inf. Proc. **11**, 1107 (2012).

[2] J. Cayssol, B. Dóra, F. Simon, and R. Moessner, Floquet topological insulators, Phys. Status Solidi RRL **7**, 101 (2013).

[3] T. Oka and S. Kitamura, Floquet engineering of quantum materials, Annu. Rev. Condens. Matter Phys. **10**, 387 (2019).

[4] F. Harper, R. Roy, M. S. Rudner, and S. L. Sondhi, Topology and broken symmetry in Floquet systems, Annu. Rev. Condens. Matter Phys. **11**, 345 (2020).

[5] M. S. Rudner and N. H. Lindner, Band structure engineering and non-equilibrium dynamics in Floquet topological insulators, Nat. Rev. Phys. **2**, 229 (2020).

[6] R. Moessner and S. L. Sondhi, Equilibration and order in quantum Floquet matter, Nat. Phys. **13**, 424 (2017).

[7] K. Sacha and J. Zakrzewski, Time crystals: A review, Rep. Prog. Phys. **81**, 016401 (2018).

[8] L. Guo and P. Liang, Condensed matter physics in time crystals, New J. Phys. **22**, 075003 (2020).

[9] D. V. Else, C. Monroe, C. Nayak, and N. Y. Yao, Discrete time crystals, Annu. Rev. Condens. Matter Phys. **11**, 467 (2020).

[10] V. Khemani, R. Moessner, and S. L. Sondhi, A brief history of time crystals, arXiv:1910.10745.

[11] F. Nathan and M. S. Rudner, Topological singularities and the general classification of Floquet-Bloch systems, New J. Phys. **17**, 125014 (2015).

[12] A. C. Potter, T. Morimoto, and A. Vishwanath, Classification of Interacting Topological Floquet Phases in One Dimension, Phys. Rev. X **6**, 041001 (2016).

[13] H. C. Po, L. Fidkowski, T. Morimoto, A. C. Potter, and A. Vishwanath, Chiral Floquet Phases of Many-Body Localized Bosons, Phys. Rev. X **6**, 041070 (2016).

[14] V. Khemani, A. Lazarides, R. Moessner, and S. L. Sondhi, Phase Structure of Driven Quantum Systems, Phys. Rev. Lett. **116**, 250401 (2016).

[15] D. V. Else and C. Nayak, Classification of topological phases in periodically driven interacting systems, Phys. Rev. B **93**, 201103(R) (2016).

[16] R. Roy and F. Harper, Periodic table for Floquet topological insulators, Phys. Rev. B **96**, 155118 (2017).

[17] S. Yao, Z. Yan, and Z. Wang, Topological invariants of Floquet systems: General formulation, special properties, and Floquet topological defects, Phys. Rev. B **96**, 195303 (2017).

[18] P. J. D. Crowley, I. Martin, and A. Chandran, Topological classification of quasiperiodically driven quantum systems, Phys. Rev. B **99**, 064306 (2019).

[19] J. Yu, R.-X. Zhang, and Z.-D. Song, Dynamical symmetry indicators for Floquet crystals, Nat. Commun. **12**, 5985 (2021).

[20] M. C. Rechtsman, J. M. Zeuner, Y. Plotnik, Y. Lumer, D. Podolsky, F. Dreisow, S. Nolte, M. Segev, and A. Szameit, Photonic Floquet topological insulators, Nature (London) **496**, 196 (2013).

[21] Y. H. Wang, H. Steinberg, P. Jarillo-Herrero, and N. Gedik, Observation of Floquet-Bloch states on the surface of a topological insulator, Science **342**, 453 (2013).

[22] G. Jotzu, M. Messer, R. Desbuquois, M. Lebrat, T. Uehlinger, D. Greif, and T. Esslinger, Experimental realization of the topological Haldane model with ultracold fermions, Nature (London) **515**, 237 (2014).

[23] W. Hu, J. C. Pillay, K. Wu, M. Pasek, P. P. Shum, and Y. D. Chong, Measurement of a Topological Edge Invariant in a Microwave Network, Phys. Rev. X **5**, 011012 (2015).

[24] S. Choi, J. Choi, R. Landig, G. Kucsko, H. Zhou, J. Isoya, F. Jelezko, S. Onoda, H. Sumiya, V. Khemani, C. von Keyserlingk, N. Y. Yao, E. Demler, and M. D. Lukin, Observation of discrete time-crystalline order in a disordered dipolar many-body system, Nature (London) **543**, 221 (2017).

[25] J. Zhang, P. W. Hess, A. Kyprianidis, P. Becker, A. Lee, J. Smith, G. Pagano, I.-D. Potirniche, A. C. Potter, A. Vishwanath, N. Y. Yao, and C. Monroe, Observation of a discrete time crystal, Nature (London) **543**, 217 (2017).

[26] W. Ma, L. Zhou, Q. Zhang, M. Li, C. Cheng, J. Geng, X. Rong, F. Shi, J. Gong, and J. Du, Experimental Observation of a Generalized Thouless Pump with a Single Spin, Phys. Rev. Lett. **120**, 120501 (2018).

[27] L. Asteria, D. T. Tran, T. Ozawa, M. Tarnowski, B. S. Rem, N. Fläschner, K. Sengstock, N. Goldman, and C. Weitenberg, Measuring quantized circular dichroism in ultracold topological matter, Nat. Phys. **15**, 449 (2019).

[28] J. W. McIver, B. Schulte, F.-U. Stein, T. Matsuyama, G. Jotzu, G. Meier, and A. Cavalleri, Light-induced anomalous Hall effect in graphene, Nat. Phys. **16**, 38 (2020).

[29] K. Wintersperger, C. Braun, F. N. Ünal, A. Eckardt, M. D. Liberto, N. Goldman, I. Bloch, and M. Aidelsburger, Realization of an anomalous Floquet topological system with ultracold atoms, Nat. Phys. **16**, 1058 (2020).

[30] P. Peng, C. Yin, X. Huang, C. Ramanathan, P. Cappellaro, Floquet prethermalization in dipolar spin chains, Nat. Phys. **17**, 444 (2021).

[31] J. Randall, C. E. Bradley, F. V. van der Gronden, A. Galicia, M. H. Abobeih, M. Markham, D. J. Twitchen, F. Machado, N. Y. Yao, and T. H. Taminiau, Many-body-localized discrete time crystal with a programmable spin-based quantum simulator, Science **374**, 1474 (2021).

[32] A. Kyprianidis, F. Machado, W. Morong, P. Becker, K. S. Collins, D. V. Else, L. Feng, P. W. Hess, C. Nayak, G. Pagano, N. Y. Yao, and C. Monroe, Observation of a prethermal discrete time crystal, Observation of a prethermal discrete time crystal, Science **372**, 1192 (2021).

[33] X. Mi, M. Ippoliti, C. Quintana, A. Greene, Z. Chen, J. Gross, F. Arute, K. Arya, J. Atalaya, R. Babbush *et al.*, Time-crystalline eigenstate order on a quantum processor, Nature (London) **601**, 531 (2022).

[34] L. Zhou and J. Gong, Non-Hermitian Floquet topological phases with arbitrarily many real-quasienergy edge states, Phys. Rev. B **98**, 205417 (2018).

[35] Z. Turker, S. Tombuloglu, and C. Yuce, PT symmetric Floquet topological phase in SSH model, Phys. Lett. A **382**, 2013 (2018).

[36] L. Zhou and J. Pan, Non-Hermitian Floquet topological phases in the double-kicked rotor, Phys. Rev. A **100**, 053608 (2019).

[37] L. Zhou, Dynamical characterization of non-Hermitian Floquet topological phases in one dimension, Phys. Rev. B **100**, 184314 (2019).

[38] L. Zhou, Non-Hermitian Floquet phases with even-integer topological invariants in a periodically quenched two-leg ladder, Entropy **22**, 746 (2020).

[39] X. Zhang and J. Gong, Non-Hermitian Floquet topological phases: Exceptional points, coalescent edge modes, and the skin effect, Phys. Rev. B **101**, 045415 (2020).

[40] H. Wu and J. An, Floquet topological phases of non-Hermitian systems, Phys. Rev. B **102**, 041119(R) (2020).

[41] L. Zhou, Y. Gu, and J. Gong, Dual topological characterization of non-Hermitian Floquet phases, Phys. Rev. B **103**, L041404 (2021).

[42] Y. Cao, Y. Li, and X. Yang, Non-Hermitian bulk-boundary correspondence in a periodically driven system, Phys. Rev. B **103**, 075126 (2021).

[43] S. Wu, W. Song, S. Gao, Y. Chen, S. Zhu, and T. Li, Floquet π mode engineering in non-Hermitian waveguide lattices, Phys. Rev. Research **3**, 023211 (2021).

[44] V. M. Vyas and D. Roy, Topological aspects of periodically driven non-Hermitian Su-Schrieffer-Heeger model, Phys. Rev. B **103**, 075441 (2021).

[45] J. Pan and L. Zhou Non-Hermitian Floquet second order topological insulators in periodically quenched lattices, Phys. Rev. B **102**, 094305 (2020).

[46] H. Wu, B. Wang, and J. An, Floquet second-order topological insulators in non-Hermitian systems, Phys. Rev. B **103**, L041115 (2021).

[47] M. van Caspel, S. E. T. Arze, and I. P. Castillo, Dynamical signatures of topological order in the driven-dissipative Kitaev chain, Sci. Post Phys. **6**, 026 (2019).

[48] L. Zhou, Non-Hermitian Floquet topological superconductors with multiple Majorana edge modes, Phys. Rev. B **101**, 014306 (2020).

[49] P. He and Z. Huang, Floquet engineering and simulating exceptional rings with a quantum spin system, Phys. Rev. A **102**, 062201 (2020).

[50] A. Banerjee and A. Narayan, Controlling exceptional points with light, Phys. Rev. B **102**, 205423 (2020).

[51] D. Chowdhury, A. Banerjee, and A. Narayan, Light-driven Lifshitz transitions in non-Hermitian multi-Weyl semimetals, Phys. Rev. A **103**, L051101 (2021).

[52] D. Chowdhury, A. Banerjee, and A. Narayan, Exceptional hexagonal warping effect in multi-Weyl semimetals, Phys. Rev. B **105**, 075133 (2022).

[53] J. Li, A. K. Harter, J. Liu, L. de Melo, Y. N. Joglekar, and L. Luo, Observation of parity-time symmetry breaking transitions in a dissipative Floquet system of ultracold atoms, Nat. Commun. **10**, 855 (2019).

[54] M. S. Rudner and L. S. Levitov, Topological Transition in a Non-Hermitian Quantum Walk, Phys. Rev. Lett. **102**, 065703 (2009).

[55] M. Chitsazi, H. Li, F. M. Ellis, and T. Kottos, Experimental Realization of Floquet PT-Symmetric Systems, Phys. Rev. Lett. **119**, 093901 (2017).

[56] L. Xiao, X. Zhan, Z. H. Bian, K. K. Wang, X. Zhang, X. P. Wang, J. Li, K. Mochizuki, D. Kim, N. Kawakami, W. Yi, H. Obuse, B. C. Sanders, and P. Xue, Observation of topological edge states in parity-time-symmetric quantum walks, Nat. Phys. **13**, 1117 (2017).

[57] X. Zhan, L. Xiao, Z. Bian, K. Wang, X. Qiu, B. C. Sanders, W. Yi, and P. Xue, Detecting Topological Invariants in Nonunitary Discrete-Time Quantum Walks, Phys. Rev. Lett. **119**, 130501 (2017).

[58] S. Weidemann, M. Kremer, S. Longhi, and A. Szameit, Topological triple phase transition in non-Hermitian Floquet quasicrystals, Nature (London) **601**, 354 (2022).

[59] L. Zhou, Floquet engineering of topological localization transitions and mobility edges in one-dimensional non-Hermitian quasicrystals, Phys. Rev. Research **3**, 033184 (2021).

[60] P. Sarnak, Spectral behavior of quasi periodic potentials, Commun. Math. Phys. **84**, 377 (1982).

[61] A. Jazaeri and I. I. Satija, Localization transition in incommensurate non-Hermitian systems, Phys. Rev. E **63**, 036222 (2001).

[62] Q. Zeng, S. Chen, and R. Lü, Anderson localization in the non-Hermitian Aubry-André-Harper model with physical gain and loss, Phys. Rev. A **95**, 062118 (2017).

[63] S. Longhi, Topological Phase Transition in Non-Hermitian Quasicrystals, Phys. Rev. Lett. **122**, 237601 (2019).

[64] T. Liu, H. Guo, Y. Pu, and S. Longhi, Generalized Aubry-André self-duality and mobility edges in non-Hermitian quasiperiodic lattices, Phys. Rev. B **102**, 024205 (2020).

[65] Q. Zeng, Y. Yang, and Y. Xu, Topological phases in non-Hermitian Aubry-André-Harper models, Phys. Rev. B **101**, 020201(R) (2020).

[66] Y. Liu, Y. Wang, Z. Zheng, and S. Chen, Exact non-Hermitian mobility edges in one-dimensional quasicrystal lattice with exponentially decaying hopping and its dual lattice, Phys. Rev. B **103**, 134208 (2021).

[67] Z. Xu and S. Chen, Dynamical evolution in a one-dimensional incommensurate lattice with PT symmetry, Phys. Rev. A **103**, 043325 (2021).

[68] X. Cai, Boundary-dependent self-dualities, winding numbers, and asymmetrical localization in non-Hermitian aperiodic one-dimensional models, Phys. Rev. B **103**, 014201 (2021).

[69] L. Tang, G. Zhang, L. Zhang, and D. Zhang, Localization and topological transitions in non-Hermitian quasiperiodic lattices, Phys. Rev. A **103**, 033325 (2021).

[70] T. Liu, S. Cheng, H. Guo, and X. Gao, Fate of Majorana zero modes, exact location of critical states, and unconventional real-complex transition in non-Hermitian quasiperiodic lattices, Phys. Rev. B **103**, 104203 (2021).

[71] L. Zhai, G. Huang, and S. Yin, Cascade of the delocalization transition in a non-Hermitian interpolating Aubry-André-Fibonacci chain, Phys. Rev. B **104**, 014202 (2021).

[72] Z.-H. Wang, F. Xu, L. Li, D. Xu, and B. Wang, Unconventional real-complex spectral transition and Majorana zero modes in nonreciprocal quasicrystals, Phys. Rev. B **104**, 174501 (2021).

[73] A. P. Acharya, A. Chakrabarty, and D. K. Sahu, Localization, PT-symmetry breaking and topological transitions in non-Hermitian quasicrystals, Phys. Rev. B **105**, 014202 (2022).

[74] X. Xia, K. Huang, S. Wang, and X. Li, Exact mobility edges in the non-Hermitian $t_1 - t_2$ model: Theory and possible experimental realizations, Phys. Rev. B **105**, 014207 (2022).

[75] H. Jiang, L. Lang, C. Yang, S. Zhu, and S. Chen, Interplay of non-Hermitian skin effects and Anderson localization in nonreciprocal quasiperiodic lattices, Phys. Rev. B **100**, 054301 (2019).

[76] S. Longhi, Phase transitions in a non-Hermitian Aubry-André-Harper model, Phys. Rev. B **103**, 054203 (2021).

[77] P. Leboeuf, J. Kurchan, M. Feingold, and D. P. Arovas, Phase-Space Localization: Topological Aspects of Quantum Chaos, Phys. Rev. Lett. **65**, 3076 (1990).

[78] R. Artuso, F. Borgonovi, I. Guarneri, L. Rebuzzini, and G. Casati, Phase Diagram in the Kicked Harper Model, Phys. Rev. Lett. **69**, 3302 (1992).

[79] T. Prosen, I. I. Satija, and N. Shah, Dimer Decimation and Intricately Nested Localized-Ballistic Phases of a Kicked Harper Model, Phys. Rev. Lett. **87**, 066601 (2001).

[80] H. Wang, D. Y. H. Ho, W. Lawton, J. Wang, and J. Gong, Kicked-Harper model versus on-resonance double-kicked

rotor model: From spectral difference to topological equivalence, Phys. Rev. E **88**, 052920 (2013).

[81] M. Lababidi, I. I. Satija, and E. Zhao, Counter-Propagating Edge Modes and Topological Phases of a Kicked Quantum Hall System, Phys. Rev. Lett. **112**, 026805 (2014).

[82] D. Y. H. Ho and J. Gong, Topological effects in chiral symmetric driven systems, Phys. Rev. B **90**, 195419 (2014).

[83] T. Shimasaki, M. Prichard, H. E. Kondakci, J. Pagett, Y. Bai, P. Dotti, A. Cao, T.-C. Lu, T. Grover, and D. M. Weld, Anomalous localization and multifractality in a kicked quasicrystal, arXiv:2203.09442.

[84] W. Gou, T. Chen, D. Xie, T. Xiao, T.-S. Deng, B. Gadway, W. Yi, and B. Yan, Tunable Nonreciprocal Quantum Transport Through a Dissipative Aharonov-Bohm Ring in Ultracold Atoms, Phys. Rev. Lett. **124**, 070402 (2020).

[85] L. Li, C. H. Lee, and J. Gong, Topological Switch for Non-Hermitian Skin Effect in Cold-Atom Systems With Loss, Phys. Rev. Lett. **124**, 250402 (2020).

[86] Z. Ren, D. Liu, E. Zhao, C. He, K. K. Pak, J. Li, and G.-B. Jo, Chiral control of quantum states in non-Hermitian spin-orbit-coupled fermions, Nat. Phys. **18**, 385 (2022).

[87] L. Zhou and W. Han, Non-Hermitian quasicrystal in dimerized lattices, Chin. Phys. B **30**, 100308 (2021).

[88] L. Zhou and Y. Gu, Topological delocalization transitions and mobility edges in the nonreciprocal Maryland model, J. Phys.: Condens. Matter **34**, 115402 (2022).

[89] W. Han and L. Zhou, Dimerization-induced mobility edges and multiple reentrant localization transitions in non-Hermitian quasicrystals, Phys. Rev. B **105**, 054204 (2022).

[90] I. Y. Goldsheid and B. A. Khoruzhenko, Distribution of Eigenvalues in Non-Hermitian Anderson Models, Phys. Rev. Lett. **80**, 2897 (1998).

[91] J. T. Chalker and B. Mehlig, Eigenvector Statistics in Non-Hermitian Random Matrix Ensembles, Phys. Rev. Lett. **81**, 3367 (1998).

[92] H. Markum, R. Pullirsch, and T. Wettig, Non-Hermitian Random Matrix Theory and Lattice QCD with Chemical Potential, Phys. Rev. Lett. **83**, 484 (1999).

[93] L. G. Molinari, Non-Hermitian spectra and Anderson localization, J. Phys. A: Math. Theor. **42**, 265204 (2009).

[94] R. Hamazaki, K. Kawabata, N. Kura, and M. Ueda, Universality classes of non-Hermitian random matrices, Phys. Rev. Research **2**, 023286 (2020).

[95] Q. Tong, J. An, J. Gong, H. Luo, and C. H. Oh, Generating many Majorana modes via periodic driving: A superconductor model, Phys. Rev. B **87**, 201109(R) (2013).

[96] R. B. Diener, G. A. Georgakis, J. Zhong, M. Raizen, and Q. Niu, Transition between extended and localized states in a one-dimensional incommensurate optical lattice, Phys. Rev. A **64**, 033416 (2001).

[97] D. J. Boers, B. Goedeke, D. Hinrichs, and M. Holthaus, Mobility edges in bichromatic optical lattices, Phys. Rev. A **75**, 063404 (2007).

[98] X. Li, X. Li, and S. Das Sarma, Mobility edges in one-dimensional bichromatic incommensurate potentials, Phys. Rev. B **96**, 085119 (2017).

[99] C. M. Dai, Y. Zhang, and X. X. Yi, Dynamical localization in non-Hermitian quasicrystals, Phys. Rev. A **105**, 022215 (2022).

[100] H. H. Yap, L. Zhou, C. H. Lee, and J. Gong, Photoinduced half-integer quantized conductance plateaus in topological-insulator/superconductor heterostructures, Phys. Rev. B **97**, 165142 (2018).

[101] I. I. Satija and A. K. Pattanayak, Non-Hermiticity in a kicked model: Decoherence and the semiclassical limit, Phys. Rev. E **65**, 045205(R) (2002).

[102] V. Goblot, A. Štrkalj, N. Pernet, J. L. Lado, C. Dorow, A. Lemaître, L. Le Gratiet, A. Harouri, I. Sagnes, S. Ravets, A. Amo, J. Bloch, and O. Zilberberg, Emergence of criticality through a cascade of delocalization transitions in quasiperiodic chains, Nat. Phys. **16**, 832 (2020).

[103] S. Roy, T. Mishra, B. Tanatar, and S. Basu, Reentrant Localization Transition in a Quasiperiodic Chain, Phys. Rev. Lett. **126**, 106803 (2021).

[104] A. Padhan, M. K. Giri, S. Mondal and T. Mishra, Emergence of multiple localization transitions in a one-dimensional quasiperiodic lattice, Phys. Rev. B **105**, L220201 (2022).